Editors' Suggestion | Featured in Physics

Optical-Relayed Entanglement Distribution Using Drones as Mobile Nodes

Hua-Ying Liu,[*] Xiao-Hui Tian,[*] Changsheng Gu,[*] Pengfei Fan,[*] Xin Ni, Ran Yang, Ji-Ning Zhang, Mingzhe Hu, Jian Guo, Xun Cao, Xiaopeng Hu, Gang Zhao, Yan-Qing Lu, Yan-Xiao Gong,[†] Zhenda Xie,[‡] and Shi-Ning Zhu[§]

National Laboratory of Solid State Microstructures, School of Electronic Science and Engineering, School of Physics, College of Engineering and Applied Sciences, and Collaborative Innovation Center of Advanced Microstructures, Nanjing University, Nanjing 210093, China

(Received 6 April 2020; accepted 1 December 2020; published 15 January 2021)

Entanglement distribution has been accomplished using a flying drone, and this mobile platform can be generalized for multiple mobile nodes with optical relay among them. Here we develop the first optical relay to reshape the wave front of photons for their low diffraction loss in free-space transmission. Using two drones, where one distributes the entangled photons and the other serves as relay node, we achieve entanglement distribution with Clauser-Horne-Shimony-Holt S parameter of 2.59 ± 0.11 at 1 km distance. Key components for entangled source, tracking, and relay are developed with high performance and are lightweight, constructing a scalable airborne system for multinode connectio and toward mobile quantum networks.

DOI: 10.1103/PhysRevLett.126.020503

Quantum communication has the potential to achieve unconditional security for information transferring, which is governed by fundamental quantum mechanics. Photons have been the most efficient carriers for the quantum information as "flying qubit," for the transmission in the quantum links in fiber [1,2] or satellites in free space [3–9]. However, fundamental challenges still remain to be resolved for building a practical quantum communication network [10,11]. Single-photon coded, the quantum link has only been established point-to-point so far, and it is critically different from classical communication, where the broadcasting-type mobile communication can be achieved using large ensembles of information replicas. Whereas there is still demand to send the quantum information among the multiple destinations, which can be ever-changing in location and time based on the requirements, regardless of the weather conditions. A more distributed architecture can fulfill this demand, using large number of nodes for the multidestination-coverage requirement, as illustrated in Fig. 1(a). Such distributed architecture calls for single cost-effective nodes and may benefit from their high flexibility and configurability for the construction of a future mobile quantum network.

Another challenge for the quantum communication is its nature of being sensitive to the link loss, which not only reduces the data rate but also criticizes on the security. The link loss seems inevitable in conventional optical communication channels like the fiber communication channels, and thus massive efforts have been devoted to the quantum repeaters. Although one can regain the security even with relatively high link loss [12–16], the data rate still drops as link loss grows. A more fundamental solution may be to reduce the total propagation loss, which requires the exploration of new communication methods. The free-space quantum communication is proposed, so that the material scattering loss can be eliminated and links can be established without fundamental low loss limit. However, the beam diffraction sets a new limit for the free-space channels, and practically the efforts to reduce the diffraction loss becomes a compromise between the beam aperture and the link distance. While lossless propagation can be achieved within Rayleigh length limit, it accumulates as the link distance scales beyond the Rayleigh length limit, as shown in Fig. 1(b). Large beam aperture helps to raise the Rayleigh length limit, but it comes with optical components in large sizes and adds weight, cost, and complexity to the node, which is especially unfavorable for large node number connections. On the other hand, optical relay may be achieved in free space, with multinodes connected in series to keep relative short link distances and still connect over a distance as required, as illustrated in Fig. 1(b). These relay nodes also become the natural hosts for the quantum repeaters to enhance the robustness of a quantum link from both approaches. Therefore, the multinode mobile connection becomes an enabling technology to resolve fundamental problems above, for the free-space quantum networks, which relies on an open question whether quantum links can be established between any of the mobile platforms, including satellites, balloons, aeroplanes, drones, etc. One of the most promising platform can be the flying drones, being fast deployable and cost effective [17,18] and capable for the construction of quantum connections at different altitudes from local-area to broad-area scales, as shown in Fig. 1(e).

In this Letter, we answer the above question and realize the first free-space link between mobile nodes for optical-

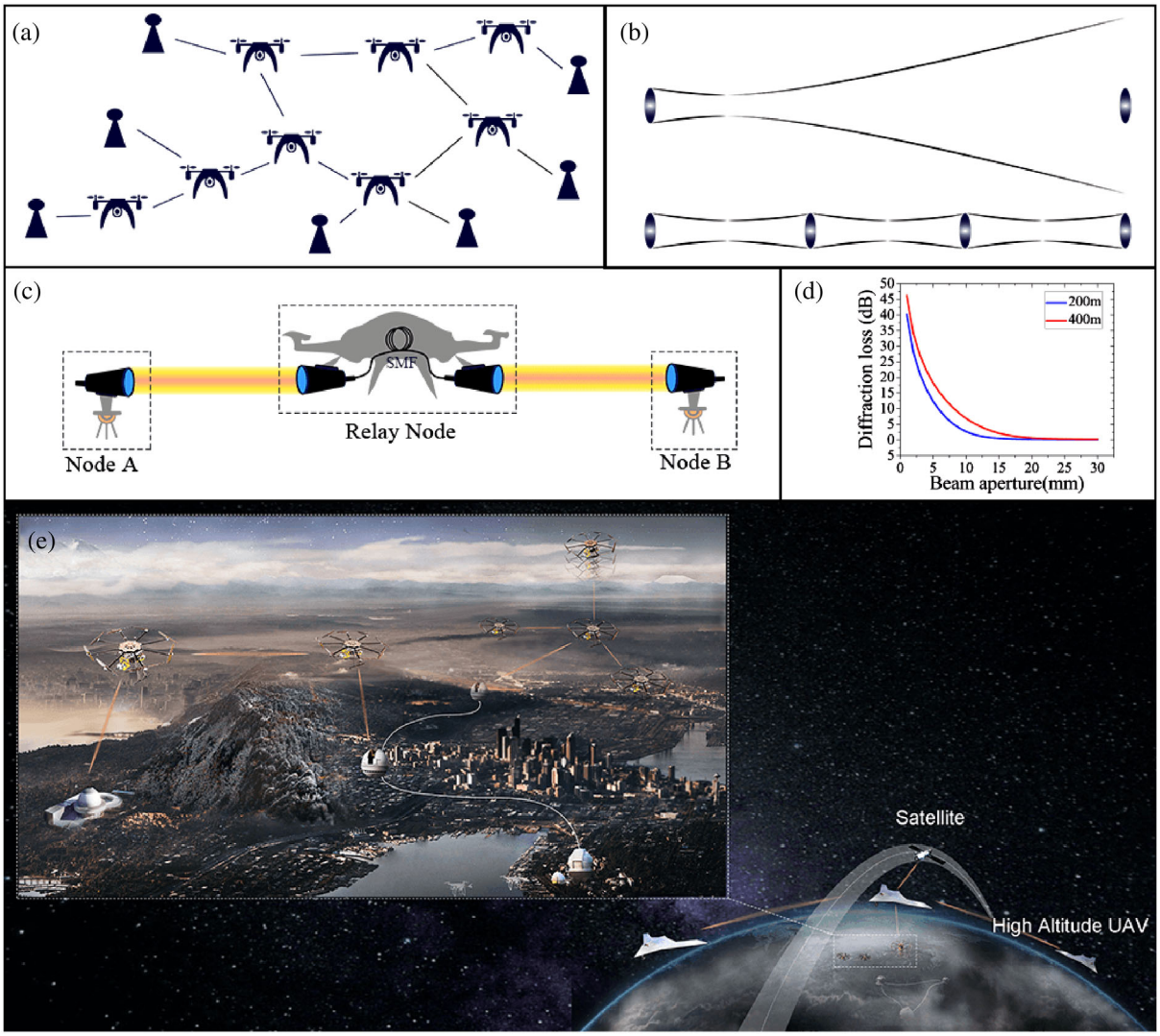

FIG. 1. Quantum network and physical realization with mobile drone-based nodes. (a) A practical quantum network consists of multinode structure and should provide access for users at any time. (b) If link distance is over the Rayleigh length limit, the beam aperture will be divergent and become larger than the receiver telescope, which inevitably brings loss to the system. Using relayed transceivers between nodes is an economical solution to keep each link distance within Rayleigh length limit to minimum the diffraction loss. (c) Diagram of the optical relay. The photon is transmitted from node A to the relay node and then retransmitted to another node B. After coupling into a SMF fiber and going through a PCS system for polarization compensation, the photons are collimated for retransmission to node B. Such diagram can be cascaded with unlimited optical relay nodes, in principle. (d) Diffraction loss versus beam aperture at link distances of 200 and 400 m, respectively, as used in our experiment. (e) Illustration scheme of a mobile quantum network using drones from local to wide-area scales. For local-area network, plug-and-play drone nodes can establish connections among mobile and fixed nodes promptly. Whereas for wide-area network, high-altitude UAVs can build multinode mobile links, which is an important supplement to the satellite and fiber-based networks.

relayed entanglement distribution. Entangled photons are generated and transmitted from one drone, and then relayed by a second drone for retransmission to the destination. Such optical relay not only steers the single-photon beam, but also reshapes its profile via single-mode-fiber (SMF) coupling and collimation against the diffraction. The distance between two destinations of Alice and Bob on the ground exceeds 1 km, with the Clauser-Horne-Shimony-Holt (CHSH) S parameter measured of 2.59 ± 0.11. Within the takeoff weight of 35 kg, a coverage time of up to 40 min is achieved for both drones. This achievement relies on multiple technological innovations, including the drones with large capacity and long flight duration, compact airborne entangled photon source (AEPS) with lightweight and high visibility, scalable airborne transceiver system, and portable ground bases.

The schematic of our optical relay is shown in Fig. 1(c). When the single-photon beam is directed toward the relay node, which is a flying drone in our case, it can be captured by a transceiver unit for the coupling into SMF. After the

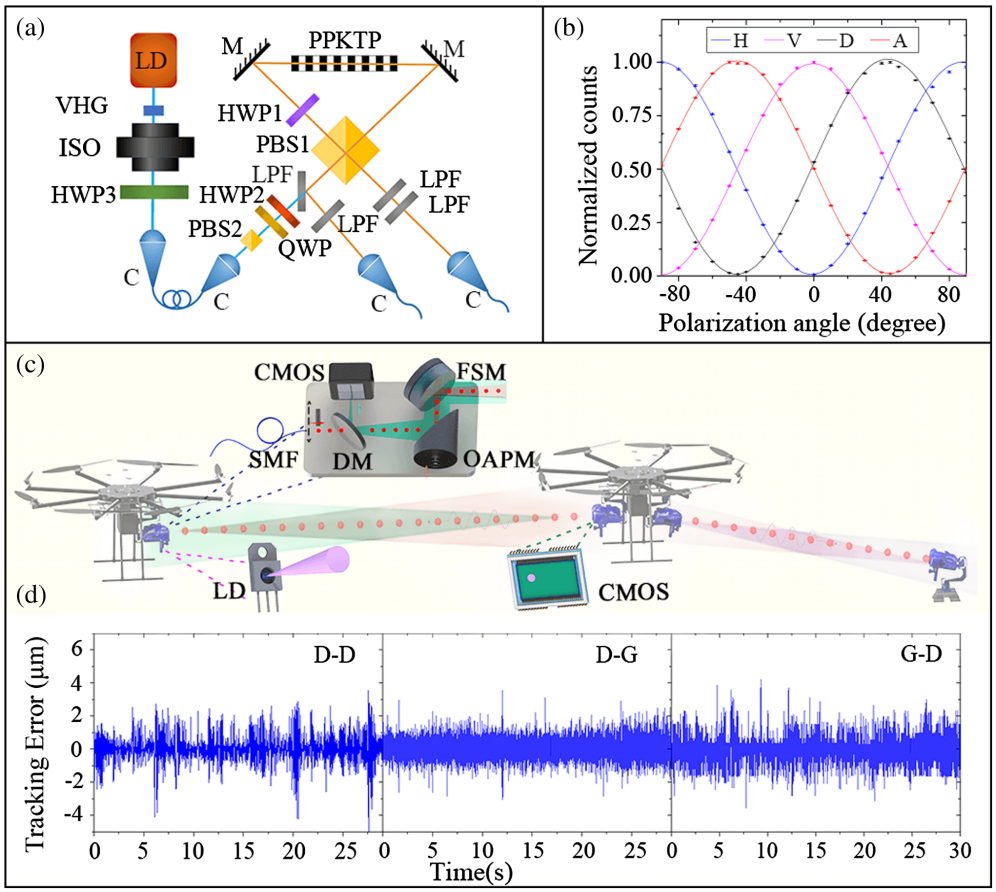

FIG. 2. Structure diagram and performance of the AEPS and the APT system. (a) Structure diagram of the AEPS. The 405 nm pump laser is a self-injection laser diode locked by a volume holography Bragg (VHG) grating. The entangled photon pair is generated by the PPKTP crystal inside a Sagnac loop. LD, laser diode; DM, dichroic mirror; ISO, isolator; LPF, long-pass filter; M, mirror; QWP, quarter-wave plate; C, collimator. (b) Two-photon correlation curves measured in lab. The interference visibilities with one photon projected to $|H\rangle$, $|V\rangle$, $|D\rangle$, and $|A\rangle$ states are 98.6%, 99.1%, 98.4%, and 98.0%, respectively. The error bars represent one standard deviation in the counts. (c) Schematic of the whole APT system. Coarse tracking is realized by a coaxial zoom camera loaded on each APT system to image the 940 nm LD of the opposite telescope. The fine tracking device is integrated inside the telescope as in the enlarged picture. CMOS, complementary metal oxide semiconductor; FSM, fast steering mirror; OAPM, off-axis parabolic mirror. (d) Tracking errors of transceivers in the 200 m drone-to-drone link and 400 m drone-ground links, respectively.

polarization compensation, the photons are directed through the SMF to the second transceiver unit for the recollimation toward the destination or the next node if necessary. Each of the transceivers is of the same design, including a telescope and its acquisition, pointing, and tracking (APT) system [19]. For the overall entanglement distribution distance of 1 km, we manage to keep the length of each link under 400 m with an optical relay, which is within the Rayleigh limit of 676 m in our system, so that the diffraction loss is negligible. Only 26.4 mm beam aperture is necessary for the telescope, which greatly reduces the size and weight of the optics, and the overall system weight as well, as shown in Fig. 1(d). As a result, we can fit both the relay node and the entanglement source node into the drones we build, which are octocopters with eight rotor legs. Their airframes are specially designed to achieve lightweight and large payload capacity (for details see Supplemental Material, Sec. I [20]).

In drone 1, the entangled photon pairs are generated from the AEPS. It is homemade via Sagnac interference [21] of a two-side pumped type-II spontaneous parametric down-conversion using a periodically poled $KTiOPO_4$ (PPKTP) crystal, as shown in Fig. 2(a). All the optics are prealigned and fixed in position with no adjustable elements, for the best in-air stability and weight control, with a light total weight of 468 g. It is capable of a photon pair generation rate of 5×10^5 Hz/mW, calculated from a coincidence measurement in lab, considering the coupling and detection efficiencies. The pump source is a homemade 405.0 nm laser and frequency degeneracy photon pairs are generated at 810.0 nm (for details, see Supplemental Material, Sec. II [20]). With the built-in set of the half-wave plate (HWP2) and the quarter-wave plate, we can control the output state of the entangled photon pairs to the following maximally polarization-entangled photon state $|\psi\rangle = (|HV\rangle_{12} - |VH\rangle_{12})/\sqrt{2}$, where $|H\rangle$ ($|V\rangle$) represents

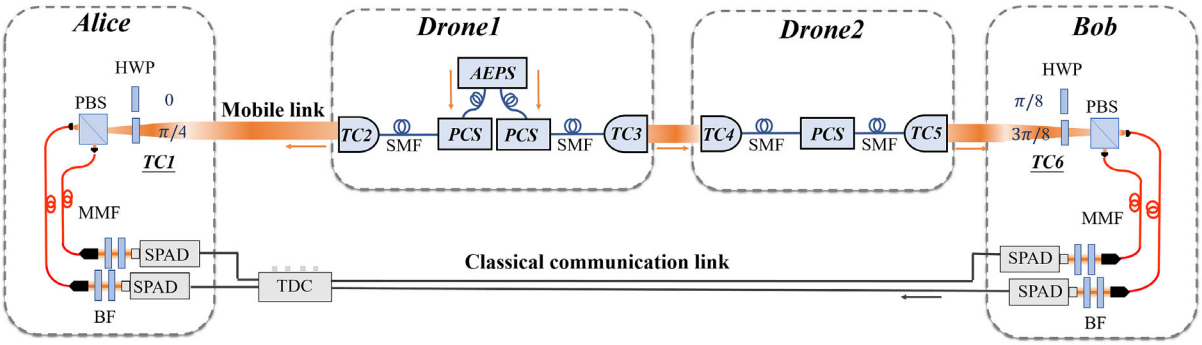

FIG. 3. The setup of the experiment. Illustration of the experimental setup for the optical-relayed entanglement distribution experiment. Drone 1 distributes the entangled photon pairs to Alice and Drone 2 (Bob) stations through mobile links. State projection measurement is performed at each ground station and a classical communication link is used for coincidence measurements. BF, band-pass filter; SPAD, single-photon avalanche detector; TC, transceiver; TDC, time-to-digital converter.

the horizontal (vertical) polarization state, and the subscripts 1 and 2 denote two output ports connecting to Alice and Bob directions, respectively. We performed four correlation measurements by projecting the photon in port 1 in $|H\rangle$, $|V\rangle$, $|D\rangle = (|H\rangle + |V\rangle)/\sqrt{2}$, and $|A\rangle = (|H\rangle - |V\rangle)/\sqrt{2}$ states, respectively, and recorded twofold coincidence counts against the linear polarization projection angles in port 2. The visibilities are measured to be 98.6%, 99.1%, 98.4%, and 98.0%, respectively, as shown in Fig. 2(b). The CHSH-type Bell inequality is also tested, with the S parameter measured to be 2.807 ± 0.006.

The photon pairs from AEPS are then directed through a polarization control system (PCS), which consists of a series of wave plates, for the correction of the polarization change in the fiber. Then they are collimated for free-space propagation and distributed through the transceiver pairs. Each transceiver is composed of a telescope platform and a three-axis motorized gimbal stage, with a total weight of 3.5 kg. The homemade system integrated in the telescope is used for the two-stage APT system. As shown in Fig. 2(c), bidirectional APT is achieved between the transceivers in a symmetric way on each side of a link. In the system, we use a fast complementary metal oxide semiconductor to detect the tracking error. Its digital output can be processed using our feedback program based on the imaging identification and digital proportional-integral-derivative loop. Noise can be filtered out and the APT system can track and retrack the target automatically when it gets lost during the flight. With the sampling frequency of 1000 Hz and the response frequency of 1000 Hz, we are able to track the target within SMF accuracy (see more details in the Supplemental Material, Sec. III [20]).

We also test the performance of the APT system in both drone-to-drone and drone-to-ground links before entanglement distribution. The tracking errors are recorded by an onboard data logging system and typical results are shown in Fig. 2(d). The tracking errors are 0.589 and 0.670 μm for the APT system on ground and drone in a 400 m drone-to-ground link and 0.697 μm for the drone APT system in a 200 m drone-to-drone link, respectively. In addition, there is an 808 nm laser diode on each drone node, which is used as the reference light and coupled in the transmitter fiber link with 1% power ratio through a 99:1 fiber coupler. It can be switched on or off remotely for link-loss measurement and real-time PCS (for details see Supplemental Material, Sec. IV [20]) or quantum measurement, respectively. Using this equipment, the free-space link losses measured from fiber to fiber are about 8 dB for the drone-to-drone link and 6 dB for the drone-to-ground link, respectively. For the drone-to-ground links, we modify the transceivers at ground stations with multimode-fiber (MMF) coupling for better stability in this first demonstration. These values are among the lowest for the free-space quantum links so far, but still high for such a system within the Rayleigh length limit. This imperfection is due to the technical loss from imperfect manual optical alignment that we use and can be reduced with better alignment strategy.

Then, we performed entanglement distribution with two mobile drones. Setup of the whole experiment is shown in Fig. 3. Entangled photons are transmitted through mobile links to ground stations (relayed drone). The entanglement is characterized by a Bell test with the CHSH-type inequality [22] between Alice and Bob, which is given by

$$S = E(a,b)\text{-}E(a,b') + E(a',b') + E(a',b') \qquad (1)$$

where $a(b)$ and $a'(b')$ are projection angles at Alice (Bob), and E is the quantum correlation between the two stations, which is measured under the projection groups $(0, 1/8\pi)$, $(0, 3/8\pi)$, $(1/4\pi, 1/8\pi)$, and $(1/4\pi, 3/8\pi)$. We used compact state projection modules at Alice and Bob stations for the measurements. Inside the ground-based transceiver, a switchable HWP set and a polarization beam splitter (PBS) are integrated in the free-space path for state projection. The switchable HWP set is used for changing the angle of projection measurement and two outputs of the PBS are the projection results under two orthogonal

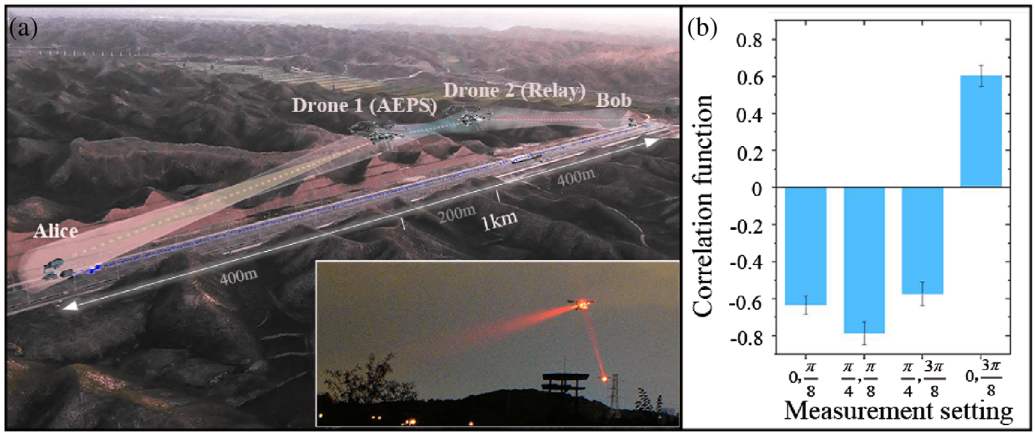

FIG. 4. Scheme and measurement results of the relayed entanglement distribution. (a) Illustration of the experimental setup for the relayed entanglement distribution experiment. Drone 1 generates the entanglement with AEPS and drone 2 collects the photons from drone 1 and retransmits them to Bob for optical relay. The distance between Alice and Bob stations exceeds 1 km. Inset: relay link in the experiment. (b) Measured correlation function results for the CHSH inequality calculation. The error bars represent 1 standard deviation in the counts.

projection bases, respectively. After the projection measurement, the single photons are collected by MMFs after going through the narrow band filter system and are connected to two single-photon avalanche diodes. The polarization extinction ratio of the whole module is over 30 dB, which is enclosed in a waterproof black box for outfield operation. Then coincident measurement is achieved between Alice and Bob through a classical optical fiber communication link, where an optical transmitter is used to convert the photon clicks from Bob's detectors to optical pulses that are then sent to Alice via fiber spools. Finally, coincidence counts are obtained at Alice through a time-to-digital converter module.

Entangled photons are generated and distributed to Alice and Bob stations, which are 1 km apart with optical relay, as shown in Fig. 4(a). The CHSH results are shown in Fig. 4(b). We collected the data for each $E(a,b)$ for 120 s and observed a signal-to-noise ratio of $\sim 20:1$. The CHSH S parameter is calculated to be 2.39 ± 0.11 without accidental subtraction or 2.59 ± 0.11 with accidental subtraction, which corresponds to a Bell inequality violation up to 5.4 standard deviations. This result is sufficient to establish mobile local-area connection in free space. With highly scalable transceiver links, such relayed quantum connection can be extended to more nodes or more complex structures for multidestinations coverage, forming a versatile local-area network (see further discussion in the Supplemental Material, Sec. V [20]).

In conclusion, we have demonstrated the first quantum link between mobile nodes using any known platform, i.e., two flying drones in this case, and optical relay is achieved for entanglement distribution. Using such mobile optical relay, we connect destination with a field-limited 1 km separation, with link length within the Rayleigh length limit that is free of diffraction loss. The optical relay geometry also allows the use of a small beam aperture of 26.4 mm, so that we can keep the total payload weight within 11.8 kg and, consequently, a take-off weight of 35 kg. CHSH S parameter is measured up to 2.59 ± 0.11 for the violation of Bell inequality by 5.4 standard deviations. Such portable system is a practical option with low cost for massive production, being suitable for the multinode architecture. Currently, the commercially available components we used have larger sizes than needed, which limits the further weight reduction of the transceivers and the drone. With further special design, we may pack a more compact system into mini-picture-drone size for local-area network or a larger beam aperture system into high-altitude unmanned aerial vehicles (UAVs) for wide-area network.

In the longer term, the structure of optical relay can be used for more than entanglement distribution, such multinode mobile link architecture can find application by hosting the quantum repeaters and rouging and multiplexing [23] the quantum information, for quantum key distribution [24], quantum teleportation [25], and quantum direct communication [26–28]. Additionally, such technology can be used in other area besides quantum communication, such as large-size distributed quantum computation [29], accurate timekeeping [30], and fundamental physics experiments such as quantum nonlocality [31] and quantum gravity [32].

The authors thank Mo Yuan, Wei Hu, Lijian Zhang, and Xiaosong Ma for helpful discussions, Fullymax Co., Ltd. for developing the high-energy density battery packs, TPpower Co., Ltd. for developing the high-performance brushless motors, and Hobbywing Co., Ltd. for custom design of the electric speed controllers. This work was supported by the National Key Research and Development Program of China (Grant No. 2019YFA0705000 and No. 2017YFA0303700), Excellent Research Program of

Nanjing University (Grant No. ZYJH002), National Natural Science Foundation of China (Grants No. 51890861, No. 11674169, No. 11621091, and No. 91321312), and the Key R&D Program of Guangdong Province (Grant No. 2018B030329001). Z. X and Y.-X. G conceived the original idea and designed the experiment. H.-Y. L., X.-H. T., C. G., P. F., X. N., R. Y., J.-N. Z., M. H. and J. G. performed the whole experiment. X. C., X. H., G. Z. and Y.-Q. L. gave advises to the experiment. All the authors helped on the manuscript preparation. Z. X., Y.-X. G. and S.-N. Z. supervised the whole work.

*These authors contributed equally to this work.
†Corresponding author.
gongyanxiao@nju.edu.cn
‡Corresponding author.
xiezhenda@nju.edu.cn
§Corresponding author.
zhusn@nju.edu.cn

[1] B. Fröhlich, M. Lucamarini, J. F. Dynes, L. C. Comandar, W. W.-S. Tam, A. Plews, A. W. Sharpe, Z. Yuan, and A. J. Shields, Long-distance quantum key distribution secure against coherent attacks, Optica **4**, 163 (2017).
[2] B. Korzh, C. Ci Wen Lim, R. Houlmann, N. Gisin, M. Jun Li, D. Nolan, B. Sanguinetti, R. Thew, and H. Zbinden, Provably secure and practical quantum key distribution over 307 km of optical fibre, Nat. Photonics **9**, 163 (2015).
[3] J. Yin *et al.*, Satellite-based entanglement distribution over 1200 kilometers, Science **356**, 1140 (2017).
[4] S.-K. Liao *et al.*, Satellite-to-ground quantum key distribution, Nature (London) **549**, 43 (2017).
[5] J.-G. Ren *et al.*, Ground-to-satellite quantum teleportation, Nature (London) **549**, 70 (2017).
[6] H. Takenaka, A. Carrasco-Casado, M. Fujiwara, M. Kitamura, M. Sasaki, and M. Toyoshima, Satellite-to-ground quantum-limited communication using a 50-kg-class microsatellite, Nat. Photonics **11**, 502 (2017).
[7] J. Yin, Y. Cao, Y. H. Li, J. G. Ren, S. K. Liao *et al.*, Satellite-to-Ground Entanglement-Based Quantum Key Distribution, Phys. Rev. Lett. **119**, 200501 (2017).
[8] X.-M. Jin *et al.*, Experimental free-space quantum teleportation, Nat. Photonics **4**, 376 (2010).
[9] R. Ursin, T. Jennewein, M. Aspelmeyer, R. Kaltenbaek, M. Lindenthal, P. Walther, and A. Zeilinger, Communications: Quantum teleportation across the Danube, Nature (London) **430**, 849 (2004).
[10] S. Wehner, D. Elkouss, and R. Hanson, Quantum internet: A vision for the road ahead, Science **362**, eaam9288 (2018).
[11] N. Gisin and R. Thew, Quantum communication, Nat. Photonics **1**, 165 (2007).
[12] Z.-S. Yuan, Y.-A. Chen, B. Zhao, S. Chen, J. Schmiedmayer, and J.-W. Pan, Experimental demonstration of a BDCZ quantum repeater node, Nature (London) **454**, 1098 (2008).
[13] H.-J. Briegel, W. Dür, J. I. Cirac, and P. Zoller, Quantum Repeaters: The Role of Imperfect Local Operations in Quantum Communication, Phys. Rev. Lett. **81**, 5932 (1998).
[14] L.-M. Duan, M. D. Lukin, J. I. Cirac, and P. Zoller, Long-distance quantum communication with atomic ensembles and linear optics, Nature (London) **414**, 413 (2001).
[15] K. Azuma, K. Tamaki, and H.-K. Lo, All-photonic quantum repeaters, Nat. Commun. **6**, 1 (2015).
[16] Z.-D. Li *et al.*, Experimental quantum repeater without quantum memory, Nat. Photonics **13**, 644 (2019).
[17] H.-Y. Liu *et al.*, Drone-based entanglement distribution towards mobile quantum networks, Natl. Sci. Rev. **7**, 921 (2020).
[18] https://www.scientificamerican.com/article/the-quantum-internet-is-emerging-one-experiment-at-a-time/.
[19] B. L. Ulich, Overview of acquisition, tracking, and pointing system technologies, Int. Soc. Opt. Photonics **887**, 40 (1988).
[20] See Supplemental Material at http://link.aps.org/supplemental/10.1103/PhysRevLett.126.020503 for details about the octocopter, the entanglement source, the APT system and the polarization compensation system, together with a brief discussion about outlook in wide-area coverage application.
[21] A. Fedrizzi, T. Herbst, A. Poppe, T. Jennewein, and A. Zeilinger, A wavelength-tunable fiber-coupled source of narrowband entangled photons, Opt. Express **15**, 15377 (2007).
[22] J. F. Clauser, M. A. Horne, A. Shimony, and R. A. Holt, Proposed Experiment to Test Local Hidden-Variable Theories, Phys. Rev. Lett. **23**, 880 (1969).
[23] S. Wengerowsky, S. K. Joshi, F. Steinlechner, H. Hübel, and R. Ursin, An entanglement-based wavelength-multiplexed quantum communication network, Nature (London) **564**, 225 (2018).
[24] H.-K. Lo, M. Curty, and K. Tamaki, Secure quantum key distribution, Nat. Photonics **8**, 595 (2014).
[25] S. Pirandola, J. Eisert, C. Weedbrook, A. Furusawa, and S. L. Braunstein, Advances in quantum teleportation, Nat. Photonics **9**, 641 (2015).
[26] G. L. Long and X. S. Liu, Theoretically efficient high-capacity quantum-key-distribution scheme, Phys. Rev. A **65**, 032302 (2002).
[27] W. Zhang, D.-S. Ding, Y.-B. Sheng, L. Zhou, B.-S. Shi, and G.-C. Guo, Quantum Secure Direct Communication with Quantum Memory, Phys. Rev. Lett. **118**, 220501 (2017).
[28] R. Qi *et al.*, Implementation and security analysis of practical quantum secure direct communication, Light **8**, 1 (2019).
[29] A. S. Cacciapuoti, M. Caleffi, F. Tafuri, F. S. Cataliotti, S. Gherardini, and G. Bianchi, Quantum internet: Networking challenges in distributed quantum computing, IEEE Network **34**, 137 (2020).
[30] P. Kómár, E. M. Kessler, M. Bishof, L. Jiang, A. S. Sørensen, J. Ye, and M. D. Lukin, A quantum network of clocks, Nat. Phys. **10**, 582 (2014).
[31] N. Brunner, D. Cavalcanti, S. Pironio, V. Scarani, and S. Wehner, Bell nonlocality, Rev. Mod. Phys. **86**, 419 (2014).
[32] P. Xu *et al.*, Satellite testing of a gravitationally induced quantum decoherence model, Science **366**, 132 (2019).